Vibrational Overtone Spectroscopy and Intramolecular Dynamics of Ethene

Alexander Portnov, Evgeny Bespechansky, and Ilana Bar*

Department of Physics, Ben-Gurion University of the Negev, Beer-Sheva 84105, Israel

Received: June 20, 2007; In Final Form: July 30, 2007

The first through fourth C−H stretching overtone regions of ethene were measured by photoacoustic spectroscopy of room-temperature molecules and action spectroscopy of jet-cooled molecules. The rotational cooling led to improved resolution in the action spectra, turning these spectra into key players in determining the multiple band appearance in each region, their types, and origins. These manifolds arise from strong couplings of the C−H stretches to doorway states and were analyzed in terms of a simplified joint local-mode/normal-mode (LM)/(NM) model and an equivalent NM model, accounting for principal resonances. The diagonalization of the LM/NM and NM vibrational Hamiltonians and the least-square fittings revealed model parameters, enabling assignment of A- and B-type bands. These bands behave differently through the $V = 2-4$ manifolds, showing coupling to doorway states for the former but not for the latter. The energy flow out of the fourth C−H overtone is governed by the interaction with bath states due to the increase in the density of states.

I. Introduction

Overtone spectra of hydride oscillators are of importance in gaining insight into vibrationally excited states of molecules and of high potential in exposing the structural and dynamical properties of molecules in their ground electronic state.[1,2] Particularly, overtone excitation facilitates monitoring of the characteristic spectral signatures, allowing retrieval of transition energies and intensities and consequently gaining of mechanistic insight on intramolecular energy flow or intramolecular vibrational energy redistribution (IVR).[3−7]

IVR is known to be a highly structured process, controlled by the coupling of a bright state to a small subset of relatively strong interacting dark background states, that is, doorway states, and successively to the high-density bath states.[4] This implies that IVR might be controlled by vibrational resonances, depending on bond type and anharmonicity, and is possibly characteristic to functional groups and transferable between molecules containing these groups. Therefore, the typical dynamics of IVR for C−H oscillators[8−21] and CH_3 groups[22−35] has been retrieved in numerous studies, some of them pointing to the importance of the Fermi resonances (trade one C−H stretch for two bend quanta). Even so, IVR can differ for each molecule, depending on the coupling strength between stretch and bend, the tuning into resonance, and the coupling with internal rotation, specifically; it might largely depend on the molecular environment of the involved group. Therefore, developing an understanding and predictability about the role of specific interactions requires studies of vibrational overtone spectra of other functional groups and particularly of C−H in additional environments.

Since hydrocarbons are central species in the field of intramolecular dynamics,[4] and the simplest olefin−ethene represents a "special case" system, where four identical C−H bonds share a C=C double-bond bridge, it would be interesting to study the vibrational pattern of this C−H chromophore. Due to the ethene size, anharmonic resonances and Coriolis-type interactions might figure extensively, resulting in complicated vibrational patterns. Although previous studies were concerned with its vibrational states,[36,37] the vibrational level structure has not been yet completely worked out. In these studies, it was found that the spectra in the $V = 1-3$ polyad regions are characterized by multiple band structure,[36,37] while those of the higher overtones are characterized by single broad features.[38−40] To improve the resolution, some of the spectra, in the 3900−7900 cm^{-1} range, were measured in a jet characterized by a rotational temperature of 53 K,[37] and those of $V = 5$ and 6 were measured at 143 K.[39] In order to reproduce the vibrational energy levels of ethene, Hamiltonian matrixes containing different diagonal and off-diagonal elements in frame of normal mode (NM)[37,38] and joint local-mode (LM)/NM models[38] were constructed.

Very recently,[41] using samples at a rotational temperature of 15 ± 2 K, we have shown by jet-cooled action spectroscopy, monitoring the yield of the released H photofragment in the ~243.1 nm photodissociation of vibrationally excited ethene as a function of the vibrational excitation wavelength, that multiple bands typify the fourth C−H stretch overtone region spectra. The partially resolved features encountered in the action spectrum together with the simulation of the spectral contours allowed determination of the band types, origins, and characteristic line widths. Accordingly, the measured action spectrum of the $V = 5$ manifold can overcome the spectral congestion in the room-temperature photoacoustic (PA) spectrum and allow one to obtain a more definitive picture concerning the existing bands.

In the present paper, we extend our measurements to the first through third C−H stretching overtone regions, while monitoring the action and the room-temperature PA spectra, and also take advantage of the $V = 5$ manifold measured spectra.[41] The action spectra benefit from reduced inhomogeneous structure due to cooling, allowing partial spectral resolution and observation of several bands in each manifold. These spectra are interpreted in terms of simplified joint LM/NM and NM models, where diagonalization of their Hamiltonian matrices results in

* To whom correspondence should be addressed. E-mail: ibar@bgu.ac.il.

10.1021/jp0748011 CCC: $37.00
Published on Web 09/22/2007

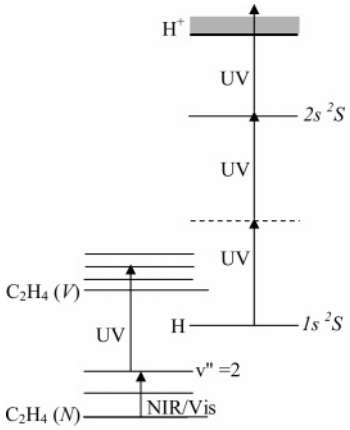

Figure 1. Schematics of the vibrationally mediated photodissociation process in ethene, showing excitation to a vibrationally excited state by visible or near-infrared photons and then promotion by ultraviolet (UV) photons to the *V* upper electronic state. The UV photons also interrogate the released H atoms, via (2 + 1) resonantly enhanced multiphoton ionization.

eigenvalues and eigenvectors. The eigenvalues are compared and fitted to the experimental band positions, allowing assignment of the observed bands. In addition, the intramolecular dynamics due to the interaction of bright states with doorway and bath states is discussed.

II. The Overtone Spectra of the C−H Stretch Regions

A. Experiment. The concept,[42,43] shown schematically in Figure 1, and the experimental setup for the vibrationally mediated photodissociation (VMP) method employed for measuring the action spectra has been described elsewhere.[44] Briefly, ethene molecules were excited to vibrationally excited states by visible (Vis) or near-infrared (NIR) photons and then promoted by ultraviolet (UV) photons to the upper electronic state. As a result of the excitation, H photofragments were released, which were interrogated by the same UV photons via ionization.

The experiments were performed in the ion source of a home-built Wiley−McLaren time-of-flight mass spectrometer (TOFMS). Two laser beams were directed into the chamber, the Vis/NIR beam for excitation of ethene to the first through fourth C−H stretch overtone regions and the UV beam for dissociation and probing. The NIR beam for excitation of the first C−H stretch overtone was provided by difference frequency mixing of the output of a pulsed dye laser, pumped by the second harmonic of a Nd:yttrium−aluminum−garnet (YAG) laser, and the residual of its fundamental. The NIR beam for excitation of the second to third overtones of the C−H stretches were provided by the idler of an optical parametric oscillator pumped by the third-harmonic output of a seeded Nd:YAG laser. The Vis beam for excitation of the fourth C−H stretch overtone was provided by the output of a tunable dye laser pumped by the second harmonic of a Nd:YAG laser. The typical pulse energies of the Vis/NIR laser were ∼0.7 μJ and ∼7, ∼11, and 40 mJ in the 1.65 and 1.13 μm and 710 and 870 nm regions, respectively. The laser pulse duration was ∼5 ns, and the line widths, as estimated from measured water lines, were 0.12 and 0.08 cm^{-1} for the first and the higher C−H overtones, respectively.

The photolysis/probe UV beam at ∼243.135 nm was generated by the doubled output of a tunable dye laser pumped by the third harmonic of another Nd:YAG and was 10 ns delayed with regard to the Vis/NIR laser. This firing sequence was repeated at a 5 or 10 Hz repetition rate. The pulse energy of the UV laser was ∼140 μJ, with a ∼5 ns duration and ∼0.2 cm^{-1} line width. The UV beam probed the H photofragments via (2 + 1) resonantly enhanced multiphoton ionization (REMPI) through the 2s $^2S \leftarrow$ 1s ^2S two-photon transition. The counterpropagating UV and Vis/NIR beams propagated perpendicularly to both the TOFMS axis and the molecular beam axis and were brought to a common focus in the center of the TOFMS ionization region.

Ethene (C_2H_4) (Aldrich, 99.5+% purity), prepared as a ∼5% mixture in Ar at a total pressure of ∼800 Torr, was expanded through an 0.8 mm orifice of a pulsed nozzle and skimmed ∼2 cm downstream of the nozzle. The molecular beam traveled another ∼3 cm to the reaction chamber center, where it was crossed by the laser beams. The typical working pressure was $\sim 5 \times 10^{-6}$ Torr, and the background pressure was about 2 orders of magnitude lower. The resulting rotational temperatures were 9−15 ± 2 K, as inferred from the action spectra simulations (see below).

Ions formed via REMPI were subjected to continuously biased extraction and acceleration stages before entering the field-free drift region and were mass selected and eventually detected by a microsphere plate or a multichannel plate. This output was fed into a digital oscilloscope and a boxcar integrator, and the H REMPI signal was then passed to a personal computer via an analog-to-digital converter and accumulated for further analysis.

Simultaneously with the action spectra, the vibrational excitation was recorded via PA spectroscopy. The pressure in the PA cell was ∼50 Torr, which led to an estimated pressure broadening of ∼0.01 cm^{-1} for the spectral lines. Wavelength calibration was accomplished by comparing the positions of the bands in the $V = 2$ region to those obtained by Herman and co-workers,[37] while for the higher overtones, is was accomplished by monitoring the water overtone transitions in the corresponding ranges via PA spectroscopy and comparing the water absorption line positions to the HITRAN database.[45]

B. The Hamiltonian Model. The approach for analyzing the spectral data and for obtaining the vibrational pattern of ethene is similar to that employed in our analysis of propyne.[33,34] This approach is based on application of simplified joint LM/NM and NM models, which were shown to be equivalent.[46−48] Therefore, we account for the principal resonances of ethene[38] and particularly keep the models equivalent through the *x*, *K* interrelations (see below).

In the simplest LM model, equivalent bonds are treated as independent anharmonic Morse-like oscillators, with a harmonic frequency of ω_m and an anharmonicity of x_m, coupled by harmonic bond interactions via the λ term. The LM matrix consists of diagonal elements of the vibrational Hamiltonian, relative to the ground state, given by the sum of local Morse oscillator energies

$$\langle n_i|H/hc|n_i\rangle = \sum_i \omega_m n_i + \sum_i x_m n_i(n_i + 1) \qquad (1)$$

where n_i are the number of quanta of excitation in the *i*th C−H stretch mode. The off-diagonal terms are related to interbond coupling due to interactions of local modes differing by one vibrational quantum in each of two equivalent bonds and are given by

$$\langle n_i,n_j|H/hc|n_i + 1,n_j - 1\rangle = \lambda[(n_i + 1)n_j]^{1/2} \qquad (2)$$

The coupling constant, λ, is given in wavenumbers and for C_2H_4 is represented by three parameters, λ_a, λ_c, and λ_t, for coupling

of adjacent, *cis*-, and *trans*-C−H bond oscillators, with respect to each other. The first bonds, related to C−H, attached to a common carbon ought to be the largest, while the last one possessing the largest distance between the C−H bonds should be the smallest[38] and was set to zero in our model due to the limited accuracy of our experiment.

In the NM description, the diagonal elements of the effective Hamiltonian matrix, which represent the vibrational energies relative to the ground vibrational states, are given by

$$\langle v_r|\hat{H}_{\text{eff}}/hc|v_r\rangle = \sum_r \omega_r v_r + \sum_{r\le s} x_{rs}\left(v_r v_s + \frac{1}{2}v_r + \frac{1}{2}v_s\right) \quad (3)$$

where ω_r are the vibrational wavenumbers of the ω_1, ω_5, w_9, and ω_{11} C−H stretch vibrations (corresponding to the ν_1 (A_g), ν_5 (B_{3g}), ν_9 (B_{2u}), and ν_{11} (B_{1u}) fundamentals)[37] and v is the number of quanta in these vibrations. The vibrational wavenumbers are related to ω_m and the coupling constants according to $\omega_1 = \omega_m + \lambda_a + \lambda_c + \lambda_t$, $\omega_5 = \omega_m - \lambda_a - \lambda_c + \lambda_t$, $\omega_9 = \omega_m - \lambda_a + \lambda_c - \lambda_t$, and $\omega_{11} = \omega_m + \lambda_a - \lambda_c - \lambda_t$. The off-diagonal elements include the Darling−Dennison interactions, which couple modes differing by two vibrational quanta in each of two different C−H stretch modes via the K_{rrss} constant

$$\langle v_r,v_s|\hat{H}_{\text{eff}}/hc|v_r+2,v_s-2\rangle = \frac{1}{4}K_{rrss}[(v_r+1)(v_r+2)v_s(v_s-1)]^{1/2} \quad (4)$$

or by one vibrational quantum, via the K_{rstu} in each of the four different C−H stretch modes

$$\langle v_r,v_s,v_t,v_u|\hat{H}_{\text{eff}}/hc|v_r+1,v_s+1,v_t-1,v_u-1\rangle = \frac{1}{4}K_{rstu}[(v_r+1)(v_s+1)v_t v_u)]^{1/2} \quad (5)$$

where v_r, v_s, v_t, and v_u correspond to the number of quanta in the C−H stretch modes.

The equivalency of the two models is obtained via the following x, K interrelations

$$x_{rr} = x_{ss} = \frac{1}{4}x_{rs} = \frac{1}{4}K_{rrss} = \frac{1}{16}K_{rstu} = \frac{1}{4}x_m \quad (6)$$

In addition, the effects of Fermi resonances in C_2H_4 are taken into account via the interaction of C−H stretches with overtones of CH_2 scissoring ($2\nu_3$, $2\nu_{12}$) and a combination of C═C stretching (ν_2) with the CH_2 scissoring mode (ν_3). The resonance of the C−H stretches with $\nu_2 + \nu_{12}$ is not considered since it is detuned over all of the measured manifolds (at $V = 2$, the detuning is 106 cm^{-1}, increasing with manifold number) and therefore not expected to contribute. In the LM basis, the Fermi resonance matrix elements are of the form

$$\langle n_i,n_j,n_k,n_l;b,c|H/hc|n_i-1,n_j,n_k,n_l;b+1,c+1\rangle = k_{ibc}[n_i(b+1)(c+1)/8]^{1/2} \quad (7)$$

$$\langle n_i,n_j,n_k,n_l;b,c|H/hc|n_i-1,n_j,n_k,n_l;b+2,c\rangle = k_{ibb}[n_i(b+1)(b+2)/8]^{1/2} \quad (8)$$

plus similar terms with i, j, k, and l permuted; b and c denote the number of quanta in CH_2 bends (scissors) and in the C═C stretch, respectively.

In the NM basis, the equivalent matrix elements are

$$\langle v_r,v_s,v_t,v_u;b,c|H/hc|v_r-1,v_s,v_t,v_u;b+1,c+1\rangle = k_{rbc}[v_r(b+1)(c+1)/8]^{1/2} \quad (9)$$

$$\langle v_r,v_s,v_t,v_u;b,c|H/hc|v_r-1,v_s,v_t,v_u;b+2,c\rangle = k_{rbb}[v_r(b+1)(b+2)/8]^{1/2} \quad (10)$$

where $k_{ibb(ibc)} = 1/2k_{rbb(rbc)}$. This scaling between the NM and LM representation is used since the ethene molecule is treated as four equivalent C−H oscillators, with the Fermi resonance constant scaling as the square of the number of oscillators.

Furthermore, the inclusion of the C═C stretch and CH_2 scissor vibrations in the models requires extension of the diagonal matrix elements to result in the following

$$\nu_C^* c + x_{CC}(c^2-c) + \nu_{b_1}b_1 + x_{b_1b_1}(b_1^2-b_1) + \nu_{b_2}b_2 + x_{b_2b_2}(b_2^2-b_2) + \sum_i x_{ic}n_i c + \sum_i x_{ib_1}n_i b_1 + \sum_i x_{ib_2}n_i b_2 + x_{cb_1}cb_1 + x_{cb_2}cb_2 + x_{b_1b_2}b_1b_2 \quad (11)$$

in the LM basis and

$$\nu_C^* c + x_{CC}(c^2-c) + \nu_{b_1b_1} + x_{b_1b_1}(b_1^2-b_1) + \nu_{b_2}b_2 + x_{b_2b_2}(b_2^2-b_2) + \sum_r x_{rc}v_r c + \sum_r x_{rb_1}v_r b_1 + \sum_r x_{rb_2}v_r b_2 + x_{cb_1}cb_1 + x_{cb_2}cb_2 + x_{b_1b_2}b_1b_2 \quad (12)$$

in the NM basis, instead of eq 3 where b_1 and b_2 are ν_3 and ν_{12}, respectively. It should be noted that ν_C^* is the effective value of the fundamental of the C═C stretch due to the Fermi coupling with $2\nu_{10}$ (C−H in-plane bending at 826 cm^{-1}).[38]

The best-fit parameters were obtained via the joint LM/NM and NM vibrational Hamiltonian matrices, which are block diagonal in the

$$V = \sum_i n_i + (c + b_1 + b_2)/2$$

and

$$V = \sum_r v_r + (c + b_1 + b_2)/2$$

manifold numbers, respectively. In addition, owing to symmetry factorization, our NM model bears only submatrices of B_{1u} and B_{2u} symmetries for each V. This is due to the fact that only transitions of these symmetries are expected in the NIR/Vis excitation of the C−H stretch manifolds. Diagonalization of the LM/NM and NM Hamiltonians result in corresponding eigenvalues and eigenvectors. Due to the structure of the bands observed in the spectra, which allow recognition of the band types (see below), the parameter fit is performed in the NM basis. The fit is carried out by comparing the eigenvalues with the observed band origins retrieved from the spectral simulations (see below). For each NM eigenvalue and eigenvector, the corresponding equivalent LM/NM values are found. These LM/NM eigenvectors allow calculation of the sum of squares of the expansion coefficients, that is, the LM character, corresponding to the pure C−H stretches in the LM basis. The fit of the eigenvalues to the band origins and the comparison of

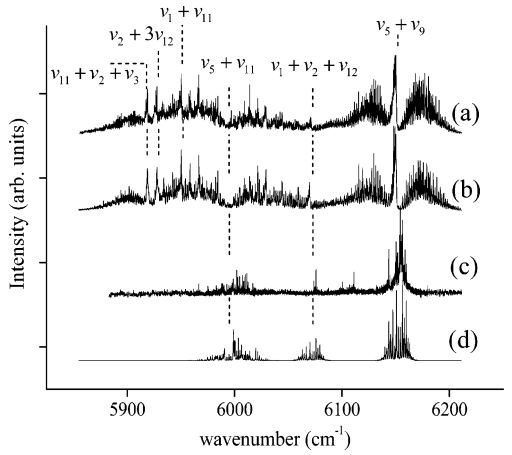

Figure 2. Vibrational overtone excitation of the first overtone of the C−H stretch region of ethene; (a) the measured room-temperature photoacoustic (PA) absorption spectrum, (b) the simulated PA spectrum, (c) the jet-cooled action spectrum monitoring the yield of H photofragments following 243.135 nm photodissociation of vibrationally excited ethene molecules and (d) the simulated action spectrum. The vertical dashed lines indicate the origins of the A- and B-type bands as obtained from the simulation. Panel (a) also includes the vibrational assignments in terms of the parameters of Table 2.

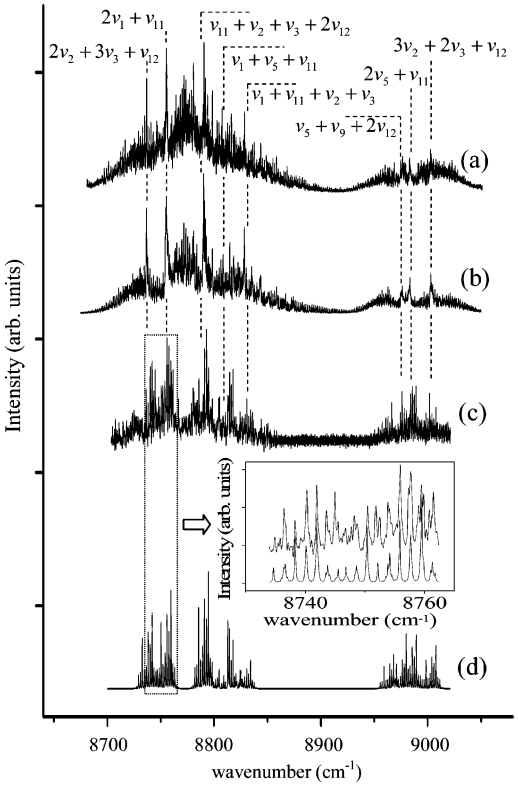

Figure 3. Vibrational overtone excitation of the second overtone of the C−H stretch region of ethene; (a) the measured room-temperature photoacoustic (PA) absorption spectrum, (b) the simulated PA spectrum, (c) the jet-cooled action spectrum monitoring the yield of H photofragments following 243.135 nm photodissociation of vibrationally excited ethene molecules, and (d) the simulated action spectrum. The vertical dashed lines indicate the origins of the A- and B-type bands as obtained from the simulation. Panel (a) also includes the vibrational assignments in terms of the parameters of Table 2. The inset shows a small portion of an expanded region of the measured (top) and simulated (bottom) action spectrum.

calculated LM character to the observed relative intensities of the dominant bands allow on to obtain the best-fit parameters via least-square analysis and assist in assigning the features.

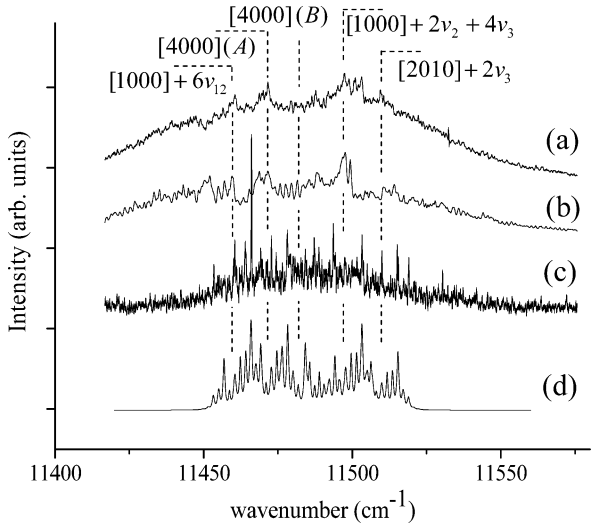

Figure 4. Vibrational overtone excitation of the third overtone of the C−H stretch region of ethene; (a) the measured room-temperature photoacoustic (PA) absorption spectrum, (b) the simulated PA spectrum, (c) the jet-cooled action spectrum monitoring the yield of H photofragments following 243.135 nm photodissociation of vibrationally excited ethene molecules, and (d) the simulated action spectrum. The vertical dashed lines indicate the origins of the A- and B-type bands as obtained from the simulation. Panel (a) also includes the vibrational assignments in terms of the parameters of Table 2.

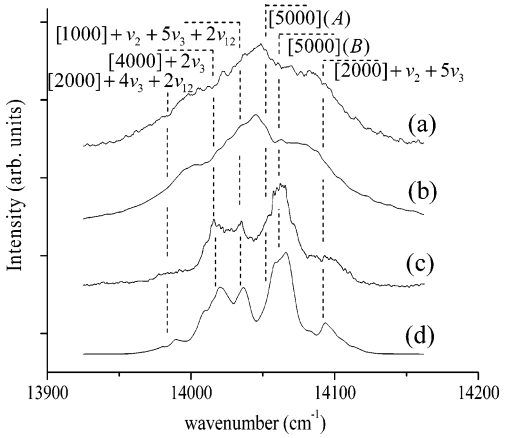

Figure 5. Vibrational overtone excitation of the fourth overtone of the C−H stretch region of ethene; (a) the measured room-temperature photoacoustic (PA) absorption spectrum, (b) the simulated PA spectrum, (c) the jet-cooled action spectrum monitoring the yield of H photofragments following 243.135 nm photodissociation of vibrationally excited ethene molecules, and (d) the simulated action spectrum. The vertical dashed lines indicate the origins of the A- and B-type bands as obtained from the simulation. Panel (a) also includes the vibrational assignments in terms of the parameters of Table 2.

III. Results

A. PA and Action Spectra. Figures 2−5 display the measured room-temperature PA spectra [panel (a)], the simulated PA spectra [panel (b)], the jet-cooled H action spectra [panel (c)], and the simulated action spectra [panel (d)] of the first through the fourth C−H stretch overtone regions of ethene. It is immediately apparent that whenever vibrational bands appear in the PA spectra [panel (a)], they are also encountered in the action spectra [panel (c)] due to enhanced photodissociation of vibrationally excited ethene molecules and successive increased H photoproduct release. Unusual is the low-frequency tail of the $V = 2$ manifold (5875−5975 cm^{-1}), where the bands, although observable in the PA spectrum, do not emerge in the action spectrum. Contrary, the band around 6104 cm^{-1} does

TABLE 1: Observed Band Positions and Assignments of the Ethene C−H Stretch Overtone Regions in Terms of the Equivalent Joint Local-/Normal-Mode and Normal-Mode Models

		assignment			
V	υ cm^{-1}	normal-mode	local-/normal-mode	type of band	obs. − calc.
2					
	5919	$\nu_{11}+\nu_2+\nu_3$	[1000][a] $+\nu_2+\nu_3$	A	−5
	5927	$\nu_2+3\nu_{12}$		A	−9
	5951	$\nu_1+\nu_{11}$	[2000]	A	0
	5995	$\nu_5+\nu_{11}$	[2000]	B	12
	6071	$\nu_1+\nu_2+\nu_{12}$	[1000] $+\nu_2+\nu_{12}$	A	−4
	6151	$\nu_5+\nu_9$	[1100]	A	−2
3					
	8736	$2\nu_2+3\nu_3+\nu_{12}$		A	11
	8754	$2\nu_1+\nu_{11}$	[3000]	A	5
	8789	$\nu_{11}+\nu_2+\nu_3+2\nu_{12}$	[1000] $+\nu_2+\nu_3+2\nu_{12}$	A	17
	8808	$\nu_1+\nu_5+\nu_{11}$	[3000]	B	24
	8829	$\nu_1+\nu_{11}+\nu_2+\nu_3$	[2000] $+\nu_2+\nu_3$	A	−1
	8975	$\nu_5+\nu_9+2\nu_{12}$	[1100] $+2\nu_{12}$	A	11
	8984	$2\nu_5+\nu_{11}$	[2100]	A	−3
	9002	$3\nu_2+2\nu_3+\nu_{12}$		A	−11
4					
	11460	$\nu_{11}+6\nu_{12}$	[1000] $+6\nu_{12}$	A	3
	11472	$\nu_1+3\nu_{11}$	[4000]	A	0
	11479	$\nu_1+\nu_9+2\nu_{11}$	[4000]	B	4
	11497	$\nu_{11}+2\nu_2+4\nu_3$	[1000] $+2\nu_2+4\nu_3$	A	−4
	11509	$3\nu_{11}+2\nu_3$	[2010] $+2\nu_3$	A	−12
5					
	13979	$\nu_5+\nu_{11}+4\nu_3+2\nu_{12}$	[2000] $+4\nu_3+2\nu_{12}$	B	−11
	14013	$\nu_5+\nu_9+2\nu_{11}+2\nu_3$	[4000] $+2\nu_3$	A	−11
	14030	$\nu_{11}+\nu_2+5\nu_3+2\nu_{12}$	[1000] $+\nu_2+5\nu_3+2\nu_{12}$	A	0
	14052	$2\nu_1+\nu_9+2\nu_{11}$	[5000]	B	−13
	14060	$\nu_1+\nu_5+\nu_9+2\nu_{11}$	[5000]	A	−3
	14090	$\nu_5+\nu_{11}+\nu_2+5\nu_3$	[2000] $+\nu_2+5\nu_3$	B	19

[a] The states $[n_1,n_2,n_3,n_4]$ correspond to n_i quanta of CH stretching in bonds which are adjacent (1,2 and 3,4), *cis* (1,4 and 2,3), and *trans* (1,3 and 2,4) with respect to each other.

not appear in the PA spectrum but is clearly noticeable in the action spectrum. Similar behavior is also encountered in the $V=3$ manifold, where a band appears at ∼8963 cm^{-1} in the action spectrum but not in the PA spectrum.

In addition, comparisons of the PA spectra to the respective action spectra show appearance of fewer rotational transitions or band contractions due to reduction of the inhomogeneous structure as a result of cooling in the latter. This behavior is most prominent in the $V=2$ manifold region, where the 6151 cm^{-1} band in the PA spectrum turns into a much narrower one in the action spectrum. Consequently, the observation of several partially resolved bands in the action spectra of each manifold allows derivation of the band origins for the respective bands. Benefiting from the retrieved origins and from the preliminary fitting of the action spectra with the JB95 asymmetric rotor program,[49] we then used the obtained molecular constants for simultaneous fitting of both the PA and action spectra by our computer code on the MATLAB application and have been able to find the observed states of Table 1, corresponding to A- and B-type bands. During the fitting procedure, the molecular constants of the ground state and the intensity alternations for ethene of 7:3:3:3 for ee, eo, oe, and oo rotational levels are constrained to their literature values.[37,50,51] To minimize the number of fitted parameters, only the molecular constants (affecting the band shape) of the excited states, the line widths, and the intensity ratios are used as fitting parameters. It should be noted that the intensity ratios between the bands appearing in each manifold of the PA spectra are found to be similar to those in the action spectra.

The obtained spectral simulations for the PA [panel (b)] and action [panel (d)] spectra of the $V=2$, 3, 4, and 5 manifolds are shown in Figures 2, 3, 4, and 5, respectively. It can be clearly seen that the fittings do not correspond very well to the respective measured spectra. For example, in the second C−H stretch overtone region, Figure 3, the simulation for the PA spectrum is reasonable, while that of the action spectrum is much poorer. This is particularly noticeable in the inset of Figure 3, showing an expanded portion of the measured (top trace) and simulated (bottom trace) action spectrum in the ∼8750 cm^{-1} region. As can be seen, the positions of the rotational transitions in the measured and fitted spectra correspond very well; however, because of the splitting of some of the lines and the non-Boltzmann distribution of the intensities, the correspondence seems to be poor. Yet, the spectral simulations of the action spectra allow one to obtain the Lorentzian line widths for the rovibrational transitions of each manifold, corresponding to 0.2 ± 0.1, 0.3 ± 0.1, 0.3 ± 0.1, and 6 ± 1 cm^{-1} for the observed features in the $V=$ 2, 3, 4, and 5 manifolds, respectively.

The band origins of the measured features of each manifold, together with the eigenvalues obtained from the LM/NM and NM Hamiltonian models, are listed in Table 1. The calculated positions are obtained using the fitted parameters of Table 2, and it is clearly observed that the measured data are reproduced quite well by these parameters. Also given in Table 1 and in Figures 2−5 [panel (a)] are the assignments of the features according to the LM/NM and NM models.

B. Intramolecular Dynamics. Some mechanistic insight into the energy flow out of the initially prepared states can be obtained by considering the density of states (DOS) in the different energetic regions. The available DOS is calculated from a harmonic oscillator model by the exact counts,[52] which gives the number of vibrational states in a certain energy interval. The fundamental frequencies of ethene have been taken from

TABLE 2: Local- and Normal-Mode Best-Fit Parameters and Uncertainties (Parentheses) in cm^{-1} for C−H Stretching Manifolds of Ethene, Accounting for Fermi Resonances[a]

LM		NM	
ω_m	3170(1)	ω_1	3137
λ_a	−45(1)	ω_5	3203
λ_c	12(1)	ω_9	3227
λ_t	0	ω_{11}	3113
x_m	−59(1)	x_{rr}	−14.75
k_{ibc}	20(2)	x_{rs}	−59
k_{ibb}	15(2)	K_{rrss}	−59
		K_{rstu}	−236
		k_{rbc}	40
		k_{rbb}	30
	ν_C^*	(1631)	
	ν_{b_1}	(1343)	
	ν_{b_2}	(1443)	
$x_{ic} = x_{ib} = x_{rc} = x_{rb} = -16$; $x_{cc} = x_{bb} = x_{cb} = -2$			

[a] Parameters in parenthesis were fixed. The normal-mode parameters were obtained using the anharmonicities and resonance parameter interrelations.

TABLE 3: Calculated Density of States (DOS) for a Particular Symmetry Species of Ethene in the Region of the $V = 2-5$ Manifolds

V	calculated DOS/cm^{-1}
2	0.2
3	1.1
4	5.3
5	18.8

ref 37. Since the ethene belongs to the D_{2h} symmetry group and the states might be of eight different symmetric species, the calculated DOS is divided by a factor of 8 to account for a statistical distribution of the states into these symmetric species. The calculated DOS for the $V = 2-5$ manifolds is given in Table 3.

IV. Discussion

A. PA and Action Spectra. The measured PA and action spectra (Figures 2 −5) and their simulations reveal the typical many-featured structure of each manifold. The spectra are characterized by A- and B-type bands only, which correspond to states of B_{1u} and B_{2u} symmetry, respectively. This can be realized by considering that ethene is an asymmetric rotor of planar geometry in the ground state, belonging to the D_{2h} point group. Provided that the rotational selection rules and thus the band types observed in the vibrational spectrum are set by the transition dipole moment of the infrared active C−H stretch bright states, it is reasonable to find components of these types only.

As pointed out above, most of the bands are observed in both the PA and action spectra; however, some of them appear in the former and not in the latter (the 5875−5975 cm^{-1} region of $V = 2$) and vice versa (the ∼6104 and 8963 cm^{-1} bands). This behavior can be explained by recalling the origins of these two types of spectra. While the PA spectra are dependent on the absorption from the ground to the vibrationally excited state, the action spectra depend also on the Franck Condon (FC) overlap with the vibrational states on the upper potential energy surface (PES) and on the transition moment to the upper electronic state.[43] The upper state is assumed to correspond to the V (π^*) state,[53] which is twisted about the C−C bond. Therefore, it seems likely that for the 5875 − 5975 cm^{-1} bands, the FC factors are relatively low and the ethene promotion to the upper rovibronic states is less effective, preventing the observation of the bands in the action spectrum at the sensitivity of our experiment. As for the ∼6104 and 8963 cm^{-1} bands appearing in the action spectrum but not in the PA spectrum, it is implied that they represent dark states, acquiring intensity during the UV excitation via improved FC factors.

Also, the nonregular intensity pattern, that is, the non-Boltzmann distribution of the intensities (see, for example, the inset of Figure 3) in the action spectra seems to be a result of the mixing of the zero-order bright states with the zero-order dark states. Indeed, rotation-induced resonances in ethene, identified and analyzed in terms of Coriolis interactions with dark states, were already suggested in previous spectroscopic studies.[36,37] These mixings might lead to different characters of the initial excitation recipients and might successively impact the brightness of the states during the second step of UV excitation via the FC factor. This is due to the fact that the excitation to the upper electronic state and the dissociation outcome might depend strongly on the components of the initially prepared states. For example, in C_2H_2[54,55] and C_2HD,[56] the mixing of specific rotational states with close zero-order dark states of bend character considerably affects the FC factors and bond fission and, most significantly, the H/D branching ratio.

In addition, it is noticed that the measured data are overall reproduced quite well by the parameter set of Table 2, allowing assignment of the observed features as shown in Figures 2−5 [panel (a)] and in Table 1. The features observed in each manifold region are related to the [V000] bright states and to the combination of the former with the CH_2 scissoring (ν_3, ν_{12}) and C═C stretching (ν_2) or their overtones, according to the resonances taken into account in the models. It is satisfying to note that all of the observed features carrying significant intensities can be assigned in the frame of these simplified LM/NM and NM models.

B. Intramolecular Dynamics. The spectra of the $V = 2-4$ manifolds and the assignment of the observed features imply that, in each region, several bands of A-type are observed but only one of B-type. For example, in the $V = 2$ manifold region, one bright state (the NM ($\nu_5 + \nu_{11}$)) is isolated, while the other ($\nu_1 + \nu_{11}$) has extensive IVR via Fermi resonances. Furthermore, by considering the splitting, $\Delta\bar{\nu}$ (cm^{-1}), between the eigenstates, the periods of energy oscillations can be obtained from the $\tau = 1/c\Delta\bar{\nu}$ relation.[11] Thus, the 200 and 24 cm^{-1} splitting between the $\nu_1 + \nu_{11}$ and the farthest away $\nu_5 + \nu_9$ and the nearest $\nu_2 + 3\nu_{12}$ states, respectively (Table 1), implies estimated redistribution time for the fastest and slowest channels of 0.08 and 0.7 ps. In the region of the fourth C−H overtone, bands of both A and B type appear, and the redistribution times to the doorway states are of ∼0.2−0.5 ps.

Moreover, the features of the region of the fourth overtone are governed by line widths of 6 ± 1 cm^{-1}, which are attributed to homogeneous broadening. As for the broadening of the states in the lower manifolds, it results from contribution of the laser line width and probably from the perturbations of the rotational lines. These perturbations result in an "effective" line width that is somewhat larger than the laser line width, but it is not attributed to homogeneous broadening. The broadening in the region of the fourth overtone is caused by the sufficient large number of states in an energetic window (18.8 states/cm^{-1}), which appear to be unresolved at our spectral resolution. This, in turn, leads to extensive energy flow to the bath states on a time scale of $\sim 0.9 \pm 0.2$ ps. This behavior is different than that obtained for the states in the lower manifolds, where the DOS (Table 3) is much lower and therefore not sufficient to cause the broadening. The ethene represents quite a unique behavior, where the DOS increases extensively only in the region of the fourth C−H stretch overtone. This is a result of

the relatively high energy fundamentals of ethene, the lower being the C−H in-plane bending at 826 cm^{-1}.[37] The estimated redistribution time for the fourth C−H stretch overtone is about the same as that of the CH_3 moiety of propyne (0.8 ± 0.2 ps)[33,34] but is much shorter than that obtained for the second acetylenic C−H overtone, $3\nu_1$, lying at 9702 cm^{-1}, which was found by Gambogi et al.[17] to be 320 ps for the $K = 0$ and 210 ps for $K = 1$ clumps and 100 ps by us.[21]

V. Conclusions

The present study is concerned with the investigation of the vibrational pattern of ethene. The first through fourth C−H stretch overtone regions were measured by room-temperature PA spectroscopy and jet-cooled action spectroscopy. On the basis of these measurements, the spectra were simulated, taking advantage of the better-resolved action spectra. These simulations allowed retrieval of the multiple-band structure of each manifold and the characteristic line widths, which were found to increase with increasing quantum number of the C−H stretch. Analysis of these multiband-structured spectra in terms of a simplified joint LM/NM model and an equivalent NM model, which accounted for the Fermi resonances with the overtones of the CH_2 scissoring ($2\nu_3$, $2\nu_{12}$) and a combination of the scissoring (ν_3) with the C=C stretch (ν_2), enabled one to obtain eigenvalues and eigenvectors. By comparison and fitting the eigenvalues to the experimental band positions and by consideration of the LM character and the observed intensity of the bands, the assignment of the observed bands could be attained (Table 1 and Figures 2−5 [panel (a)]). Furthermore, some mechanistic insight regarding energy flow out of the initially excited C−H stretches was obtained. The B_{1u} and B_{2u} symmetry bright states, respectively, behaved differently through the $V = 2-4$ manifolds, showing coupling to doorway states for the former but not for the latter. The initial energy flow out of the B_{1u} states was to the doorway states via Fermi resonances and occurred on subpicosecond time scales. Of particular importance is the fact that the DOS for the $V = 2-4$ manifolds was not sufficient to be pronounced by the measured line widths under our resolution. On the other hand, for $V = 5$, the higher DOS caused extensive homogeneous broadening, which reflected the energy decay out of the C−H stretches of the fourth overtone to the bath states.

Acknowledgment. The authors gratefully acknowledge support by the James Franck Binational German−Israeli Program in Laser-Matter Interaction and by the Israel Science Foundation founded by The Israel Academy of Science and Humanities.

References and Notes

(1) Henry, B. R. *Acc. Chem. Res*. **1987**, *20*, 429.
(2) Henry, B. R.; Kjaergaard, H. G. *Can. J. Chem*. **2002**, *80*, 1635.
(3) Gruebele, M.; Wolynes, P. G. *Acc. Chem. Res.* **2004**, *37*, 261.
(4) Beil, A.; Luckhaus, D.; Quack, M.; Stohner, J. *Ber. Bunsen-Ges. Phys. Chem. Chem. Phys*. **1997**, *101*, 311.
(5) Nesbitt, D. J.; Field, R. W. *J. Phys. Chem*. **1996**, *100*, 12735.
(6) Lehmann, K. K.; Scoles, G.; Pate, B. H. *Annu. Rev. Phys. Chem*. **1994**, *45*, 241.
(7) Quack, M. In *Mode Selective Chemistry*; Jerusalem Symposium; Jortner, J., Levine, R. D., Pullman, B., Eds.; Kluwer Academic Publishers: Dordrecht, The Netherlands, 1991; Vol. 24, p 47.
(8) Davidsson, J.; Gutow, J. H.; Zare, R. N.; Hollenstein, H. A.; Marquardt, R. R.; Quack, M. *J. Phys. Chem*. **1991**, *95*, 1201.
(9) Segall, J.; Zare, R. N.; Dubal, H. R.; Lewerenz, M.; Quack, M. *J. Chem. Phys*. **1987**, *86*, 634.
(10) Amrein, A. H.; Dubal, H. R.; Quack, M. *Mol. Phys*. **1985**, *56*, 727.
(11) Boyarkin, O. V.; Settle, R. D. F.; Rizzo, T. R. *Ber. Bunsen-Ges. Phys. Chem. Chem. Phys.* **1995**, *99*, 504.
(12) Melchior, A.; Chen, X. L.; Bar, I.; Rosenwaks, S. *J. Phys. Chem*. A **2000**, *104*, 7927.
(13) Li, L. B.; Dorfman, G.; Melchior, A.; Rosenwaks, S.; Bar, I. *J. Chem. Phys*. **2002**, *116*, 1869.
(14) (a) Callegari, A.; Merker, U.; Engels, P.; Srivastava, H. K.; Lehmann, K. K.; Scoles, G. *J. Chem. Phys*. **2000**, *113*, 10583. (b) Callegari, A.; Merker, U.; Engels, P.; Srivastava, H. K.; Lehmann, K. K.; Scoles, G. *J. Chem. Phys*. **2001**, *114*, 3344.
(15) Gambogi, J. E.; Lesperance, R.; Lehmann, K. K.; Scoles, G. *J. Phys. Chem*. **1994**, *98*, 5614.
(16) McIlroy, A.; Nesbitt, D. J.; Kerstel, E. R. T.; Pate, B. H.; Lehmann, K. K.; Scoles, G. *J. Chem. Phys*. **1994**, *100*, 2596.
(17) (a) Gambogi, J. E.; Kerstel, E. R. Th.; Lehmann, K. K.; Scoles, G. *J. Chem. Phys*. **1994**, *100*, 2612. (b) Gambogi, J. E.; Timmermans, J. H; Lehmann, K. K.; Scoles, G. *J. Chem. Phys*. **1993**, *99*, 9314.
(18) McIlroy, A.; Nesbitt, D. J. *J. Chem. Phys*. **1994**, *101*, 3421.
(19) Go, J.; Cronin, T. J.; Perry, D. S. *Chem. Phys*. **1993**, *175*, 127.
(20) Yoo, H. S.; DeWitt, M. J.; Pate, B. H. *J. Phys. Chem*. A **2004**, *108*, 1348.
(21) Ganot, Y.; Rosenwaks, S.; Bar, I. *J. Chem. Phys*. **2005**, *122*, 244318.
(22) Duncan, J. L.; New, C. A.; Leavitt, B. *J. Chem. Phys*. **1995**, *102*, 4012.
(23) Law, M. M. *J. Chem. Phys*. **1999**, *111*, 10021.
(24) Kjaergaard, H. G.; Rong, Z. M.; McAlees, A. J.; Howard, D. L.; Henry, B. R. *J. Phys. Chem. A* **2000**, *104*, 6398.
(25) Rong, Z. M.; Kjaergaard, H. G. *J. Phys. Chem*. A **2002**, *106*, 6242.
(26) Cavagnat, D.; Lespade, L. *J. Chem. Phys*. **1998**, *108*, 9275.
(27) Cavagnat, D.; Lespade, L. *J. Chem. Phys*. **2001**, *114*, 6030.
(28) Cavagnat, D.; Lespade, L. *J. Phys. Chem*. A **2005**, *109*, 4062.
(29) Henry, B. R.; Turnbull, D. M.; Schofield, D. P.; Kjaergaard, H. G. *J. Phys. Chem*. A **2003**, *107*, 3236.
(30) Chen, X.; Melchior, A.; Bar, I.; Rosenwaks, S. *J. Chem. Phys*. **2000**, *112*, 4111.
(31) Melchior, A.; Chen, X.; Bar, I.; Rosenwaks, S. *J. Chem. Phys*. **2000**, *112*, 10787.
(32) Dorfman, G.; Melchior, A.; Rosenwaks, S.; Bar, I. *J. Phys. Chem*. A **2002**, *106*, 8285.
(33) Portnov, A.; Bespechansky, E.; Ganot, Y.; Rosenwaks, S.; Bar, I. *J. Chem. Phys*. **2005**, *122*, 224316.
(34) Portnov, A.; Blockstein, L.; Bar, I. *J. Chem. Phys*. **2006**, *124*, 164301.
(35) Portnov, A.; Ganot, Y.; Bespechansky, E.; Rosenwaks, S.; Bar, I. *Vib. Spectrosc*. **2006**, *42*, 147.
(36) (a) Oomens, J.; Oudejans, L.; Reuss, J.; Fayt, A. *Chem. Phys*. **1994**, *187*, 57. (b) Oomens, J.; Reuss, J.; Mellau, G. C.; Klee, S.; Gulaczyk, I.; Fayt, A. *J. Mol. Spectrosc*. **1996**, *180*, 236.
(37) (a) Georges, R.; Bach, M.; Herman, M. *Mol. Phys*. **1999**, *97*, 279 and references therein. (b) Bach, M.; Georges, R.; Herman, M.; Perrin, A. *Mol. Phys.* **1999**, *97*, 265.
(38) Duncan, J. L.; Ferguson, A. M. *J. Chem. Phys.* **1988**, *89*, 4216.
(39) Crofton, M. W.; Stevens, C. G.; Klenerman, D.; Gutow, J. H.; Zare, R. N. *J. Chem. Phys*. **1988**, *89*, 7100.
(40) Sension, R. J.; Mayne, L.; Hudson, B. *J. Am. Chem. Soc*. **1987**, *109*, 5036.
(41) Bespechansky, E.; Portnov, A.; Zwielly, A.; Rosenwaks, S.; Bar, I. *J. Chem. Phys.* **2006**, *125*, 133301.
(42) Crim, F. F. *J. Phys. Chem*. **1996**, *100*, 12725.
(43) Bar, I.; Rosenwaks, S. *Int. Rev. Phys. Chem*. **2001**, *20*, 711.
(44) Portnov, A.; Ganot, Y.; Rosenwaks, S.; Bar, I. *J. Mol. Struct*. **2005**, *744*, 107.
(45) Rothman, L. S.; Jacquemart, D.; Barbe, A.; Benner, D. C.; Birk, M.; Brown, L. R.; Carleer, M. R.; Chackerian, C., Jr.; Chance, K.; Coudert, L. H.; Dana, V.; Devi, V. M.; Flaud, J.-M.; Gamache, R. R.; Goldman, A.; Hartmann, J.-M.; Jucks, K. W.; Maki, A. G.; Mandin, J.-Y.; Massie, S. T.; Orphal, J.; Perrin, A.; Rinsland, C. P.; Smith, M. A. H.; Tennyson, J.; Tolchenov, R. N.; Toth, R. A.; Vander Auwera, J.; Varanasi, P.; Wagner, G. Jr. The 2004 HITRAN Molecular Spectroscopic Database and HAWKS (HITRAN AtmosphericWorkstation); Atomic and Molecular Physics Division, Harvard-Smithsonian Center for Astrophysics. *J. Quant. Spectrosc. Radiat. Transfer* **2005**, *96*, 139.
(46) Mills, I. M.; Robiette, A. G. *Mol. Phys*. **1985**, *56*, 743.
(47) Lehmann, K. K. *J. Chem. Phys*. **1986**, *84*, 6524.
(48) Law, M. M.; Duncan, J. L. *Mol. Phys*. **1998**, *93*, 821.
(49) Plusquellic, D. F. *JB95 Spectral Fitting Program*; http://physics.nist.gov/ Divisions/Div844/facilities/uvs/overview.html.
(50) Rusinek, E.; Fichoux, H.; Khelkhal, M.; Herlemont, F.; Legrand, J.; Fayt, A. *Mol. Phys.* **1998**, *189*, 64.
(51) Herzberg, G. *Infrared and Raman Spectra of Polyatomic Molecules, MolecularSpectra and Molecular Structure*; Van Nostrand Reinhold: New York, 1945; Vol. II.
(52) (a) *MultiWell-2.08 Software*; designed and maintained by Barker, J. R., with contributions from Ortiz, N. F.; Preses, J. M.; Lohr, L. L.;

Maranzana, A.; Stimac, P. J. University of Michigan: Ann Arbor, MI, 2007; http://aoss.engin.umich.edu/multiwell/. (b) Barker, J. R. *Int. J. Chem. Kinet.* **2001**, *33*, 232.

(53) (a) Merer, A. J.; Mulliken, R. S. *Chem. Rev.* **1969**, *69*, 639. (b) Mulliken, R. S. *Phys. Rev.* **1932**, *41*, 751. (c) Mulliken, R. S. *Phys. Rev.* **1933**, *43*, 297. (d) Wilkinson, P. G.; Mulliken, R. S. *J. Chem. Phys.* **1955**, *23*, 1895.

(54) Sheng, X.; Ganot, Y.; Rosenwaks, S.; Bar, I. *J. Chem. Phys.* **2002**, *117*, 6511.

(55) Ganot, Y.; Golan, A.; Sheng, X.; Rosenwaks, S.; Bar, I. *Phys. Chem. Chem. Phys.* **2003**, *5*, 5399.

(56) Arusi-Parpar, T.; Schmid, R. P.; Li, R.-J.; Bar, I.; Rosenwaks, S. *Chem. Phys. Lett.* **1997**, *268*, 163.